POLITECNICO DI TORINO

Dipartimento di Ingegneria Meccanica e Aerospaziale

Corso di Laurea Magistrale in Ingegneria Aerospaziale

Tesi di Laurea Magistrale

Validation by wind-tunnel experimentation of aeromechanical models.

Relatori
prof. Paolo Maggiore
ing. Matteo Davide Lorenzo Dalla Vedova

Candidato
Federico Pagano

October 15
2019

Contents

Riassunto

Il presente lavoro si ripromette di analizzare l'effetto della deformazione torsionale di ali a freccia marcata sul controllo dell'equilibratore.
Ciò deriva da un sempre maggiore utilizzo, nelle costruzioni aeronautiche, di ala a allungamento elevato e freccia marcata, costruita in materiali compositi. Questa scelta è volta al miglioramento dell'efficienza aerodinamica nell'ottica di una riduzione di costi e consumi.
Questo tipo di geometria alare, tuttavia, è soggetta ad ampie deformazioni quando posta sotto carico. Anche rimanendo lontani dai fenomeni di divergenza strutturale, il comportamento aerodinamico cambia secondo la deformazione subita dalla struttura. Pertanto il pilota o il sistema di comando dovrà compensare questa differenza di comportamento tra il caso rigido e il caso flessibile.
In questo senso è stato sviluppato uno schema di calcolo per iniziare a modellizzare il fenomeno sotto alcune importanti semplificazioni. Successivamente è stato progettato e costruito un modello fisico ricalcante le caratteristiche di quello teorico e sono state fatte delle prove in galleria del vento.
Il modello è impostato con uno schema formato da due sezioni principali che costituiscono una semiala. Una sezione si trova fissata alla fusoliera mentre l'altra è fissata a una barra di torsione collegata a una molla che simula tutta la flessibilità torsionale in modo concentrato. La sezione mobile può essere scalata rispetto a quella fissa in modo da poter simulare ali a freccia positiva, diritta e negativa.
Il lavoro si è parecchio concentrato nella definizione dell'attrezzatura sperimentale. Alcuni dati sono stati raccolti, ma particolare attenzione è stata posta al collaudo delle soluzioni tecniche per poter gettare le basi di lavori futuri.

Chapter 1

Introduction

The needing to increase the optimization of the air transportation system, especially in terms of fuel consumption, is today a well recognised priority in aerospace engineering. This is related to a number of factors such as costs for operators and enviromental matters for emissions.
Nowadays some high-performance materials are available and this let airplane project engineers to adopt an high aspect ratio and high sweeping angle for wing design. This, as well known, increases the aerodynamic efficiency.
Composites have very high performances under stress, but despite they are strong in strenghtness, the high aspect ratio of the wing is not a very stiff structure, so high deformations are normally achieved. The enormous amount of studies made by universities and industries all over the world ensure the safety of high deformations of composite wings.
Deformation modifies the aerodynamic behaviour of the wing. Also in this case aeroelasticity science can predict accurately divergence and flutter, very dangerous instability phenomenon of structures.
However, also in normal conditions, structure flexibility can alter the manovrability of the airplane, compared to the perfectly stiff ideal situation.
Wing flexibility effects can affect the control system (or pilots reactions) also so far from critical instability problems. Control surfaces in the flexible case must reach a deflection angle different from the rigid condition.
This work aims to investigate the effects of the torsional deformation of swept wings on elevator control in static conditions.
Considering a conventional airplanes configuration, as well known, for a certain angle of attack of the plane, at equilibrium the elevator must produce a lift in order to keep null the total moment on the plane.
Consider a positive or negative swept wing with high aspect ratio value: the lift along the wing span produces a bending and a torsional moment. The first simplification, for our purposes, is to consider the torsional moment only, because is the only that affects the longitudinal wing moment amount. In facts, to the torsional moment corresponds an elastic deformation of the wing, more specifically a rotation of wing sections. This means that considering a flexible wing instead of a rigid one, the angle of attack of wing sections changes as a function of the global angle of attack and the wingspan position. As a conseguence the total wing moment is different between the rigid and the flexible cases and the equilibrator must reach a different angle to fullfill his function.
This effect is different considering a positive or negative swept wing, so we will analyze the phenomenon for this two cases.
The torsional divergence cases well known, but a reliable model of the effect of wing elasticity over equilibrator, also for normal working condition, could be useful to develop a more efficient control system.
The worst case is the negative swept angle. For a negative swept wing configuration the lift

along wing span tends to rotate wing sections increasing the local angle of attack. As a conseguence lift locally increases and pitch moment too. The torsional deformation should increase with speed and angle of attack. At a certain speed the deformation is so high that the elevator can't compensate the resulting moment. This is the worst case and it is important to avoid this flight condition that would be catastrophic.

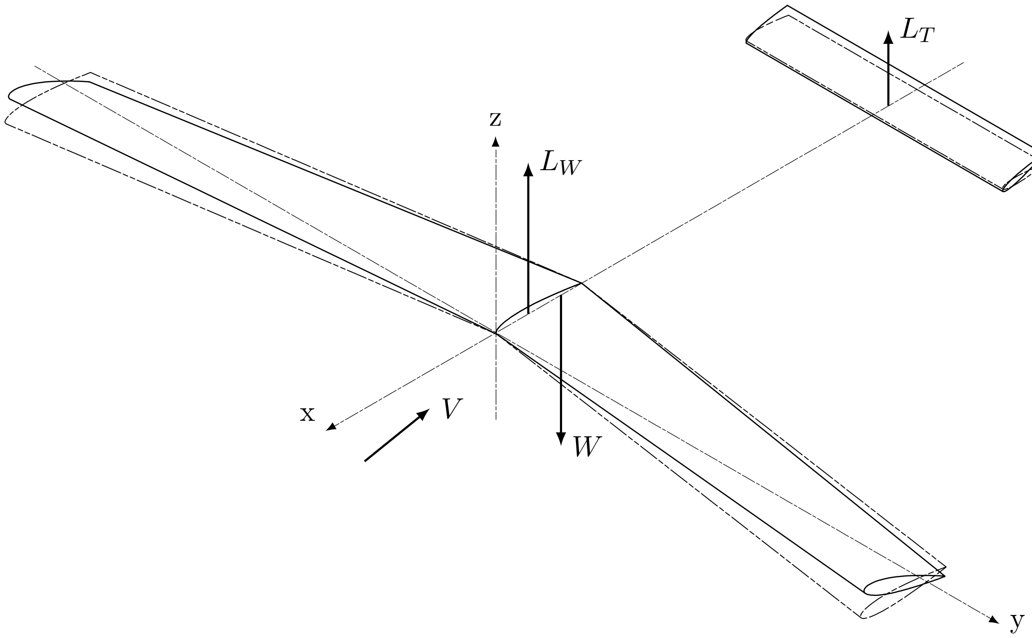

Figure 1.1: Loads diagram on a generic airplane with a negative swept wing configuration. A qualitative deformation of wing tips is shown.

Chapter 2

Theoretical Model

2.1 General Configuration

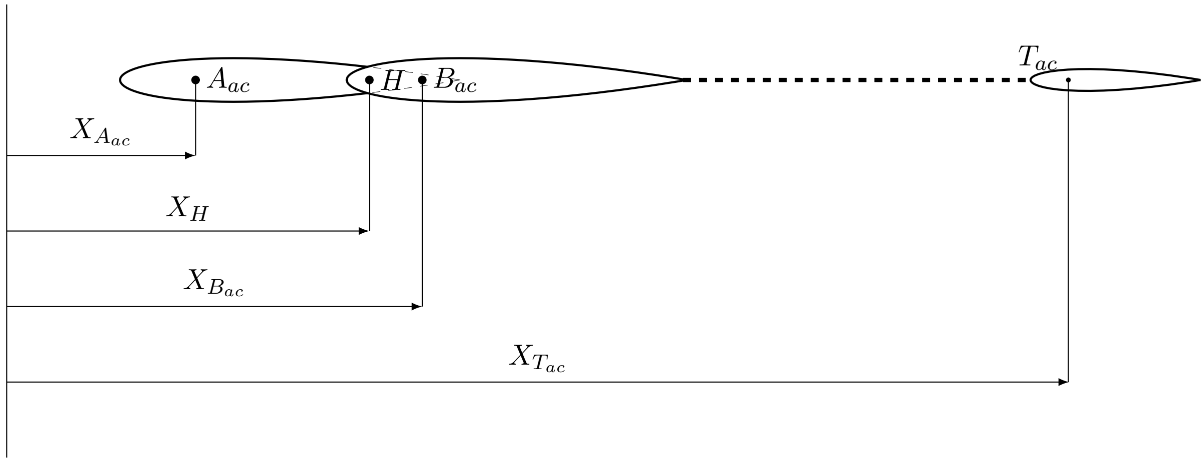

Figure 2.1: A_{ac} B_{ac} and T_{ac} are the aerodynamic centers of the respective surfaces. H is the hinge point.

This chapter reports the theoretical analysis of the phenomenon. The main task is to compare the elevator angle required to provide static stability to a plane in case of rigid or flexible wing. The focus is posed on the (positive or negative) swept wing due to the torsional effects of the lift that are coming with this architecture.
The analytic model will be developed considering the same situation of the physical model will be tested in the wind tunnel. The model will be mounted with the wing-span axis oriented in vertical direction, avoiding the influence of center of gravity to longitudinal stability. The center of gravity influence will be considered in the theoretical model and will be considered virtually in the test model, searching on load cells a moment correspondant to opposite of the weight ammount instead of null moment.
In order to investigate the phenomenon a simplified wing model is considered. The torsional stiffness of the whole wing is intended as concentrated in a single point in the middle of the wing span. Reffering to the Figure 2.1, the wing is modelled by two elements: a fixed one (A) for the inner part and a moveable one (B) for the outer part. The two parts are linked by a torsion spring hinge. The fixed part is linked rigidly to a body that allows the transmission of the loads from the wing to the tail (T).The mutual positions of the moveable wing, the fixed wing, the tail, and the spring hinge can be changed to consider different plane configurations: straight wing, positive or negative swept wing. From this initial assumptions a mathematical model is developed.

The distances of the aerodynamic centers and the hinge point are given from an arbitrary datum.

2.2 Load Path

2.2.1 Loads on section B

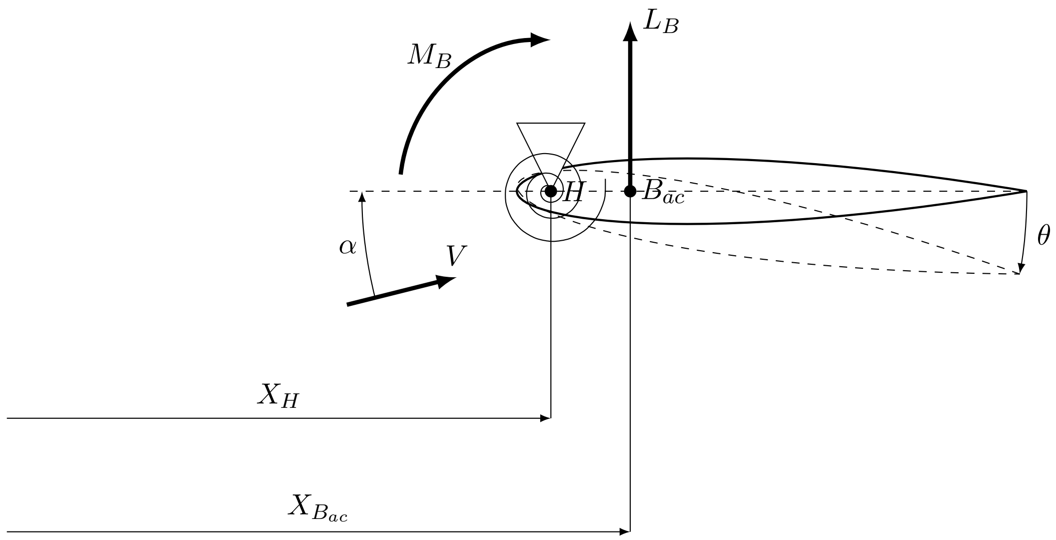

Figure 2.2: Detail of isolated B section.

As shown in the Figure 2.2, the torque loads applied to the flexible section around the H hinge are an airfoil characteristic aerodynamic moment M_B, a moment due to the lift L_B and a elastic restoring moment due to the spring. Drag effects are considered as negligible.
The spring is linked to the fixed and the moveable part of the wing, k_θ is the spring stiffness. The θ angle is defined between the relaxed position of the spring (B chord aligned to A) and the generic rotated position of B.
The angle of attack α is referred to the fixed wing. So the angle of attack of the moveable wing is considered equal to $\alpha + \theta$. The equation coming from the equilibrium of moments for the section B is:

$$M_B - L_B \cdot (X_{B_{ac}} - X_H) - k_\theta \cdot \theta = 0 \tag{2.1}$$

From the (2.1), the moment M_{BA} transferred from the section B to the section A through the point H is:

$$M_{BA} = k_\theta \cdot \theta = M_B + L_B \cdot (X_H - X_{B_{ac}}) \tag{2.2}$$

A vertical force is applied in H to the section A, it is considered equal to L_B.

2.2.2 Loads on section A and static equilibrium of complete plane.

The section A is affected from its own aerodynamic loads and from the loads coming from the section B, as previously evaluated. Considering the aerodynamic center of the section A as the pole of the moments, the moment on the plane coming from the whole wing is:

$$M_{wing} = M_{BA} + M_A - L_B \cdot (X_H - X_{A_{ac}}) \tag{2.3}$$

For the static equilibrium of the whole plane, the elevator lift L_T has to balance only the wing moment and the moment given by the weight[1]. The equilibrium equation is simply:

$$M_{wing} - L_T \cdot (X_{T_{ac}} - X_{A_{ac}}) - W \cdot (X_W - X_{A_{ac}}) = 0 \tag{2.4}$$

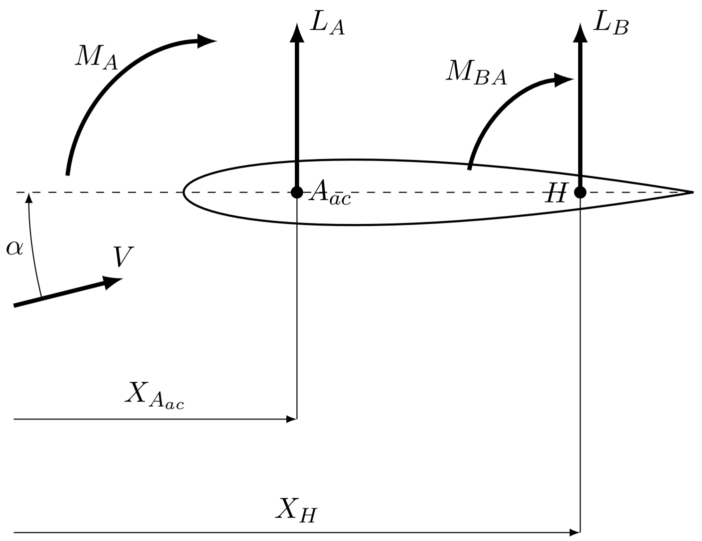

Figure 2.3: Detail of isolated A section.

For each angle of attack α, a value of the rotation angle θ and elevator angle δ_T have to be found.

2.3 Formulation with Aerodynamic Coefficients

2.3.1 Section A

For the fixed wing section, the following lift and moment formulations are used:

$$L_A = \frac{1}{2}\rho V^2 S_A C_{L_{\alpha A}} \cdot \alpha \tag{2.5}$$

$$M_A = \frac{1}{2}\rho V^2 S_A c_A C_{M_A} \tag{2.6}$$

2.3.2 Section B

For the movable wing section, the following lift and moment formulations are used:

$$L_B = \frac{1}{2}\rho V^2 S_B C_{L_{\alpha B}} \cdot (\alpha + \theta) \tag{2.7}$$

$$M_B = \frac{1}{2}\rho V^2 S_B c_B C_{M_B} \tag{2.8}$$

Replacing this formulations the (2.1) become:

$$k_\theta \cdot \theta = \frac{1}{2}\rho V^2 S_B c_B C_{M_B} + \frac{1}{2}\rho V^2 S_B C_{L_{\alpha B}} \cdot (\alpha + \theta) \cdot (X_H - X_{B_{ac}}) \tag{2.9}$$

[1]The reader can remark that in a standard aeromechanical formulation all the forces and moments are referred to the center of mass, so seems to be improper to define a "moment of the weight". In our case the test model will rotate around the fixed wing center of pressure axe. So the center of mass gives a moment to consider.

Expliciting θ:

$$\theta = \frac{\frac{1}{2}\rho V^2 S_B c_B C_{M_B} + \frac{1}{2}\rho V^2 S_B C_{L_{\alpha B}} \cdot \alpha \cdot (X_H - X_{B_{ac}})}{k_\theta - \frac{1}{2}\rho V^2 S_B C_{L_{\alpha B}} \cdot (X_H - X_{B_{ac}})} \tag{2.10}$$

It is now possible to formulate the global forces and moment generated by the wing as function of θ and aerodynamic coefficients.
So replacing aerodynamic coefficient in (2.2) the moment M_{BA} transmitted from B to A is:

$$M_{BA} = \frac{1}{2}\rho V^2 S_B c_B C_{M_B} + \frac{1}{2}\rho V^2 S_B C_{L_{\alpha B}} \cdot (\alpha + \theta) \cdot (X_H - X_{B_{ac}}) \tag{2.11}$$

2.3.3 Equilibrator

It is now possible to use this relations in the previous equation to obtain total moment (2.3). This moment should be opposed from the equilibrator action. Expliciting the equilibrator lift from the (2.4) we can write:

$$L_T = \frac{M_{wing} + W \cdot (X_W - X_{A_{ac}})}{(X_{T_{ac}} - X_{A_{ac}})} \tag{2.12}$$

Introducing aerodynamic coefficient also for equilibrator:

$$L_T = \frac{1}{2}\rho V^2 S_T C_{L_{\alpha T}} \cdot (\alpha + \delta_T) \tag{2.13}$$

It is possible to obtain the equilibrator angle:

$$\delta_T = \frac{L_T}{\frac{1}{2}\rho V^2 S_T C_{L_{\alpha T}}} - \alpha \tag{2.14}$$

2.4 Results

The theoretical model developed here can be used to produce results for many configurations. To make easy a direct comparison we present here the results for the same configurations achievable by the real model.
Due to technical needs during construction of the real model, the hinge positions for the flexible part are four, corresponding to four holes. These are made respectively at 12.5%,25%, 37.5%, and 50% of the airfoil chord. In the fixed part the hinge is at 25% of the chord. This means we have only a positive swept wing configuration (12.5%), a straight wing configuration (25%), and two negative swept wing configurations (37.5%, and 50%).

Chapter 3

Test Model Design

This chapter reports the mechanical designation of test model to be used in the wind tunnel. The task is to explore the behaviour of the model by tests, having the same kind of input and output data of the theoretical model to make comparisions. A CAD system is used to evaluate solutions.

3.1 Preliminary Design

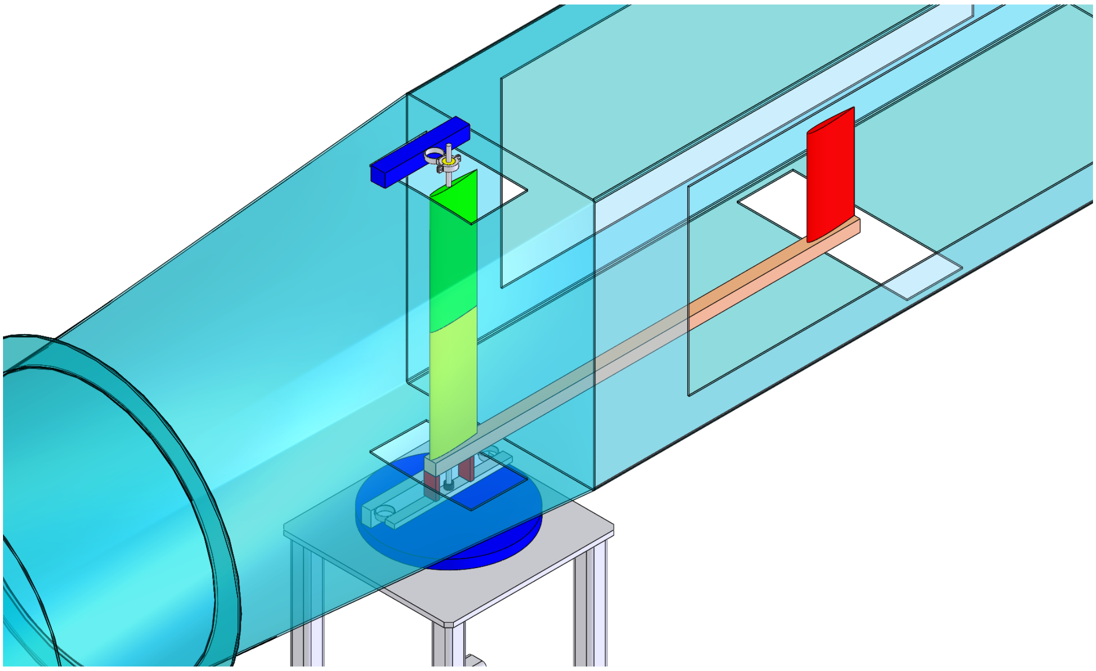

Figure 3.1: Test model preliminary layout.

A preliminary design was done by evaluating general sizes of the available test chamber. In order to have a better wing aspect ratio and better access to the test chamber we decided to have a vertical configuration as shown in figure 3.1.
As for the theoretical model, we have two main wing sections: the inner (in yellow) is fixed to the body, and the outer (in green) it is movable and it drives the spring placed in the basement by a torsion rod passing free through the inner wing section.
The tail wing (red), even if vertical, is the elevator and it is mounted on the body, moved by an actuation system that is still under study at this time.
The sensor system is supposed to be formed by three load cells. Two of them placed in a

crankcase structure under the test chamber, and the third over the chamber. This configuration should provide data about the total lift (as sum of the three load cells) and the total moment (as the difference of the two cells in the crankase times the arm among them).
So we need to measure the lift (L) and the wing moment (M) as a function of load cells signal.

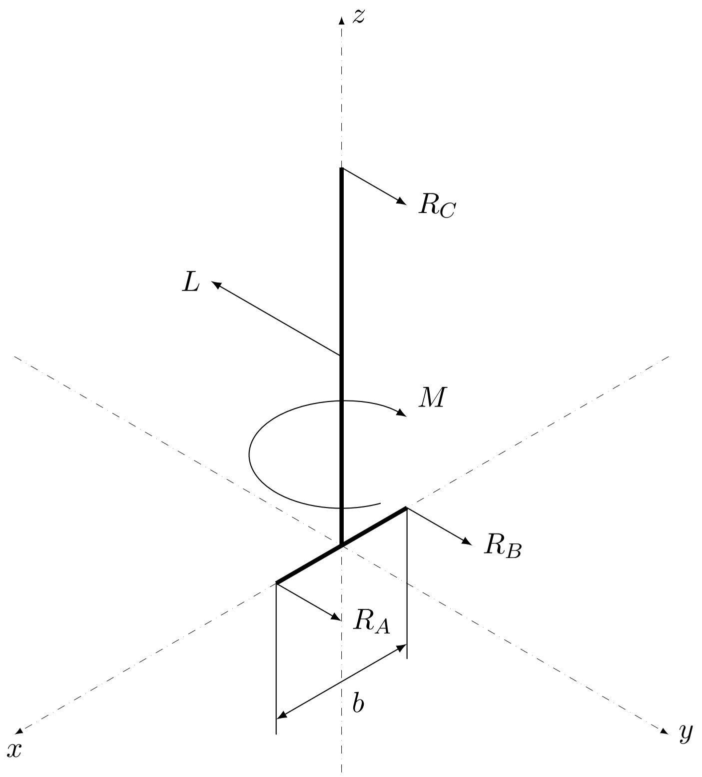

Figure 3.2: Schematic diagram of loads on the model. Reactions R corresponds to load cells signals.

The equilibrium equations written according to Figure 3.2 are:

$$\begin{cases} (\Rightarrow)\ \Sigma F_y = 0 \\ (\circlearrowleft)\ \Sigma M_z = 0 \end{cases} \Longrightarrow \begin{cases} L - R_A - R_B - R_C = 0 \\ M - (R_B - R_A) \cdot b = 0 \end{cases}$$

And expliciting aerodynamic loads:

$$\begin{cases} L = R_A + R_B + R_C \\ M = (R_B - R_A) \cdot b \end{cases}$$

Therefore, for what has been said, an important matter is the number of deegrees of freedom contrained from each element of the sensor system. We are going to study technical solutions to constrain with cells only the degrees of freedom related to forces that should be measured, and to constrain with structure all other degrees, with particular attention to cross correlation (mutual influence between degrees of freedom). Structure must do not over constrain the system. We wil see the technical solutions to acheve that in the next section.

3.2 Final Design

The final design is composed of a wooden joist as the rigid body. Two wing sections are printed in plastic material. The inner is rigidly linked to the joist, the outer is fixed with two nuts on a threaded bar.

The threaded bar bring to the balance the torsion torque generated from the upper wing section to the spring that is fixed the torsion balance, while the joist is directly linked. In the tail the equilibrator is moved by a servomotor.
Let's now see every part in detail.

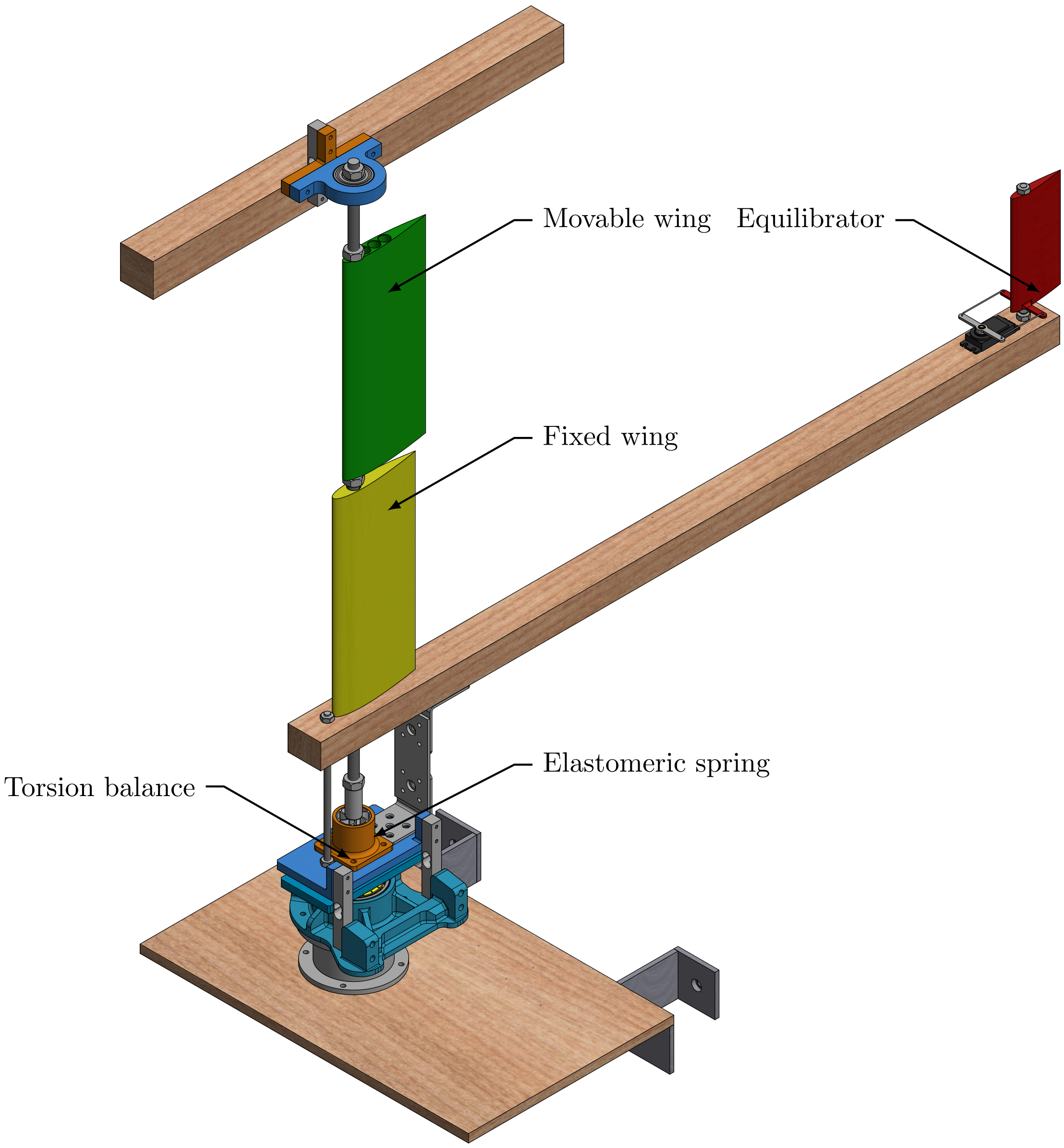

Figure 3.3: General overview of the test model assembly.

3.2.1 Main wing

The main wing is composed by two sections printed in `PETG` plastic with a 3D printer. The fixed section is provided with an hole to let the threaded bar to pass through without contact and it is fixed to the joist.
The outer section is mounted on the threaded bar and it is fixed by a couple of nuts. The threaded bar is fixed outside the test chamber with a bearing hinge that leaves free the rotation on the vertical axis. The bearing hinge is linked to the load cell, and we obtain the signal R_C (see Figure 3.2). In the bottom section the threaded bar is linked with a support fixed with

epoxydic glue to the center of elastomeric hinge.
The total moment amount is composed by the sum of the fixed and the movable wing sections and it is transferred to the balance.
The movable section is provided with four holes that allow the locking of the wing in different position. Holes are respectively at 12.5%,25%,37.5% and 50% of the span.

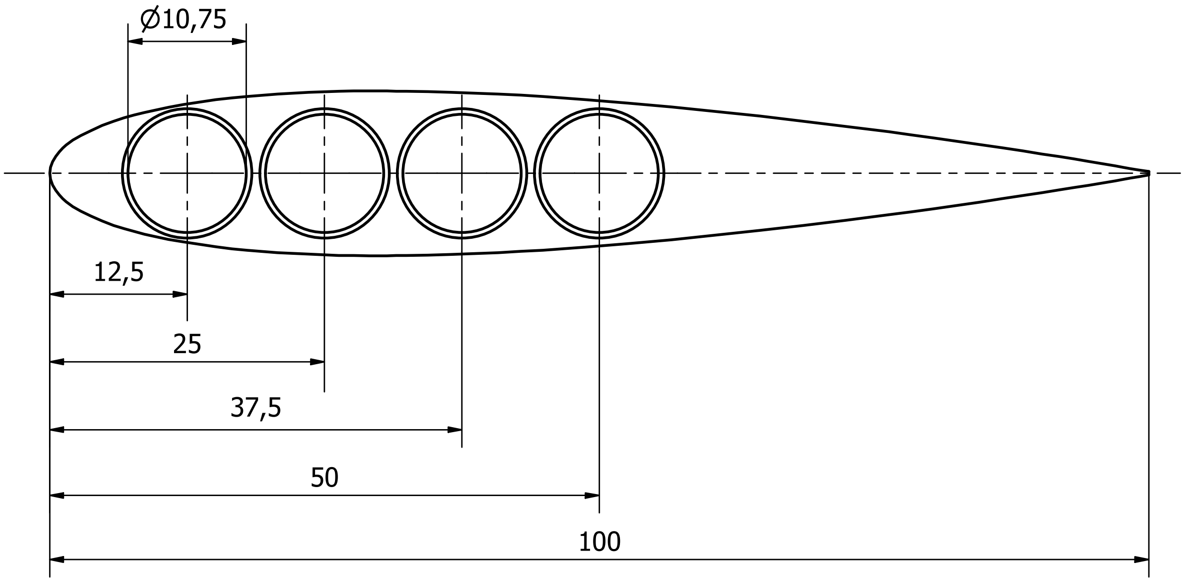

Figure 3.4: Detail of the movable wing with holes for assembly in different positions.

3.2.2 Equilibrator

The equilibrator is located in the tail section, at the opposite end of the wooden joist. A threaded bar is fixed with nuts thru the joist and the wing section is free to rotate on it. In the wing section, also printed in `PETG`. On the sides of the wing section, two arms are built and linked to the servo motor shaft, in a articulated quadrilateral configuration.
The servo motor is controlled by an Arduino board that provide to increase the deflection angle of the equilibrator until the momento on load cells is correct.

3.2.3 Elastomeric Hinge

CAD design

An elastomeric hinge is needed to provide the elastic behaviour to simulate the torsional stiffness of the wing. In order to support the weight of the movable section and radial forces, this part should be also a frictionless bearing system.
At first a CAD model was developed and used to print the part with elastomeric material. Then tests took place to have a stress-deformation characterization of the part.
The part is intended to work with the external wall fixed to a support linked to the basement and the internal wall fixed to an insert linked to the torsion bar (figure 3.6).

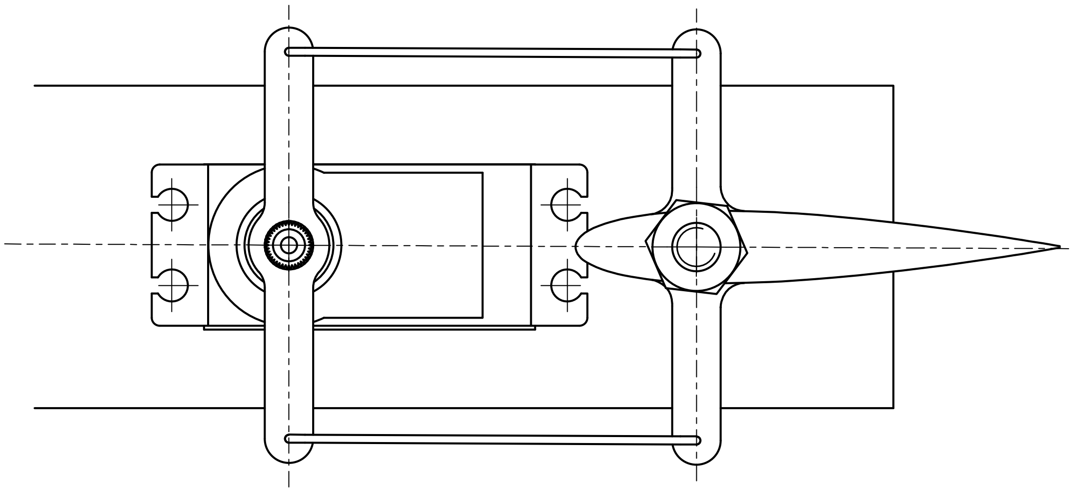

Figure 3.5: Equilibrator actuation system.

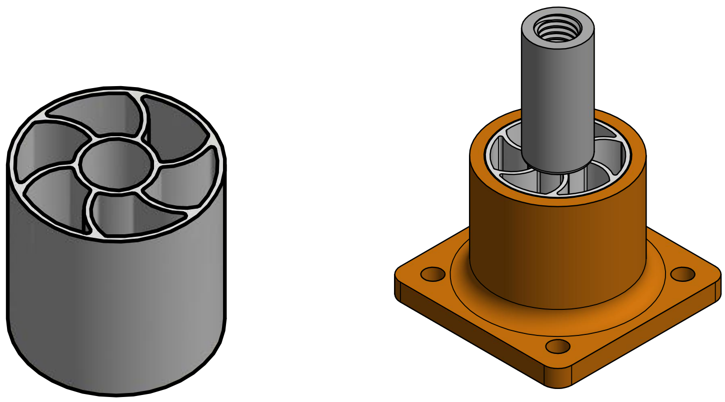

Figure 3.6: Elastomeric bearing CAD model with supports for linking.

Charaterization

A torsion balance was designed and built with available material to define the stress deformation curve of the elastomeric hinge.
A bike wheel is fixed to a torsion bar to work as a pulley. An inextensible rope is fixed to the pulley to link different value of mass. As the mass values and the radius of the pulley are known it is possible to impose torque values to the elastomeric hinge.
The most accurate way we found to mesure deformation angles was taking photos of wheel spokes from a fixed position. A 2D CAD system was used to measure relative angles from the photos.

3.2.4 Test balance

A test balance is designed to measure the lift and the pitching moment. Remembering that the model is mounted with the wing span in the vertical direction, the real weight of the structure must not be taken into account. Also the drag component is not measured. So the main task of the test balance is to measure the wanted forces and to be strongly numb to others. So a

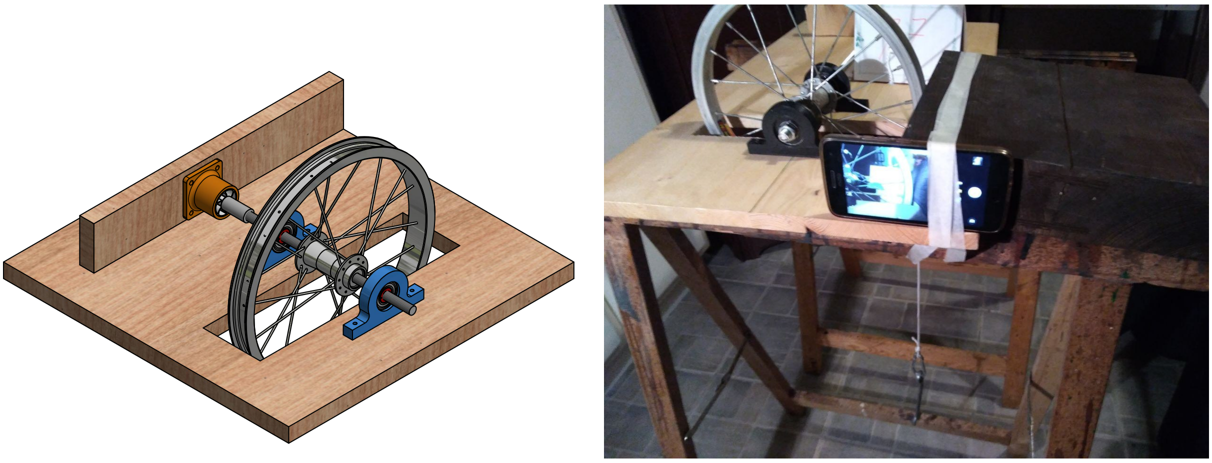

Figure 3.7: On the left the torsion balance CAD model. On the right the torsion balance during tests. Loads are linked to the cable and deformation is measured taking photos from a fixed point.

structure is projected to keep the model in position. Load cells stop only degrees of freedom corresponding to the measured forces.
So the balance is designed with a rolling table that leaves free the translation on the horizontal axis. A bearing leaves free also rotation around threaded bar axis. In this way load cells can stop the degrees of freedom corresponding to R_A and R_B as seen in the figure 3.2. The model proper weight and the drag component are taken from the structure and don't affect the load cells signals.

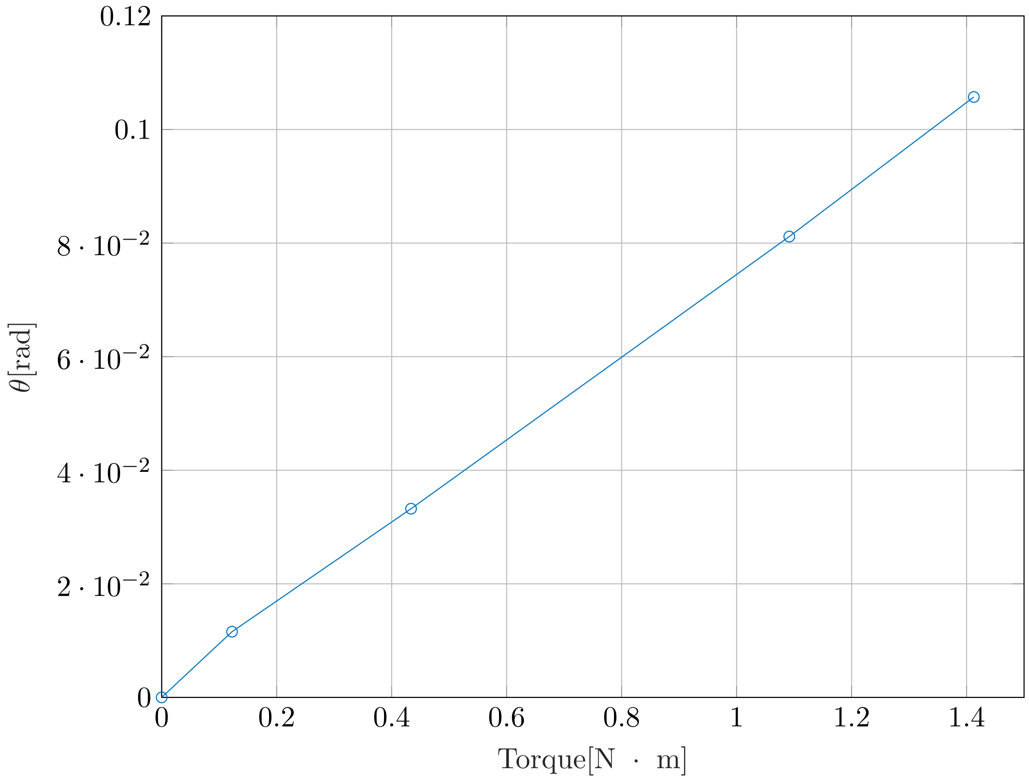

Figure 3.8: Load/Deformation diagram for the elastomeric hinge.

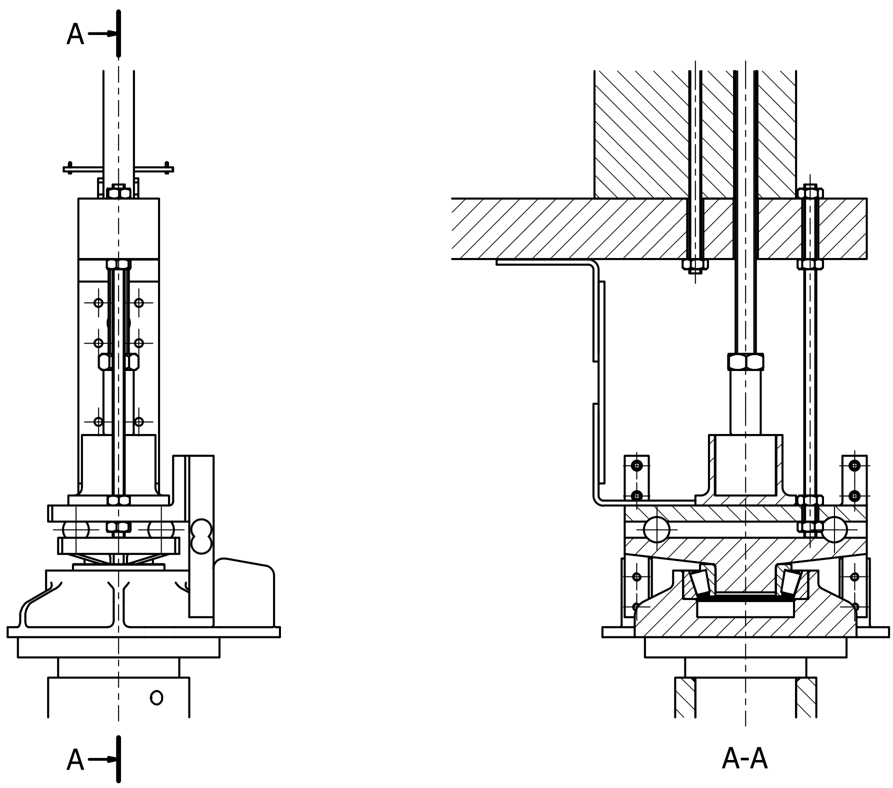

Figure 3.9: Torsion balance CAD model.

Chapter 4

Tests

4.1 Instruments and facilities

4.1.1 Wind tunnel plant

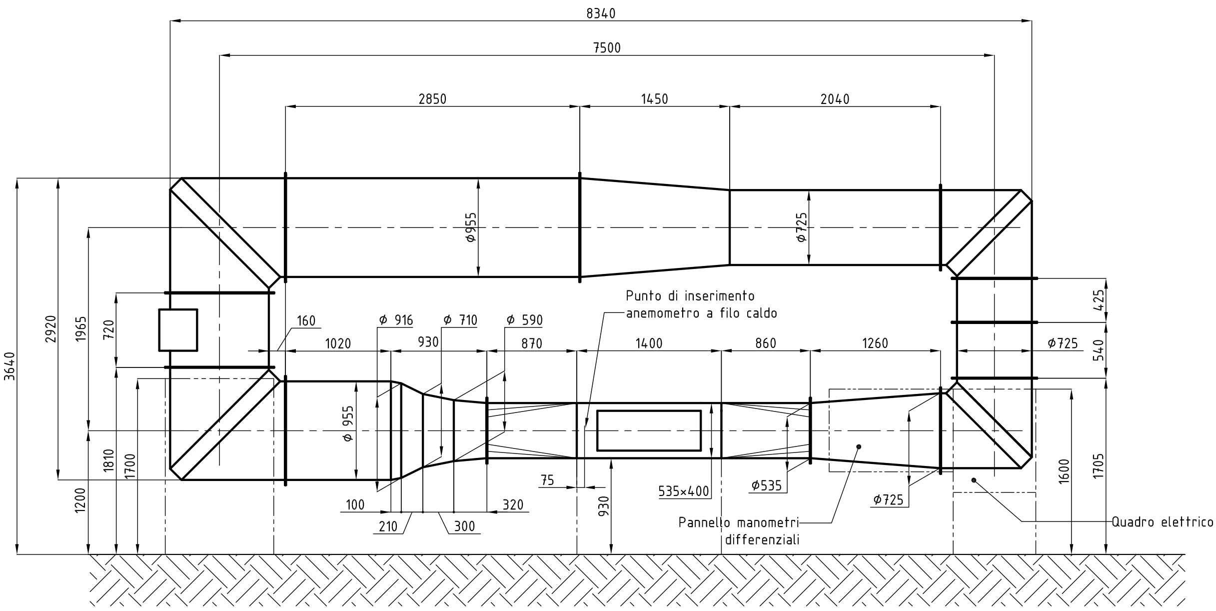

Figure 4.1: General dimensions of the wind tunnel plant

The wind tunnel used for tests is located at ITIS A. Volta, in Alessandria. The general dimensions are shown in figure 4.1. Built in the middle of '80s, the plant is a close circuit tunnel with a closed test section.
A modern electronic system developed in Labview takes care of the air speed control. This consists in a hot wire anemometer and a PID controller. A three phases electric motor drive a constant speed fan. The controller is working on some fins that regulate the airflow increasing and decreasing the flow section near after the fan. This system provides an air speed tolerance on the nominal value of 0.1 m/s. The available range of speed is from 6 to 50 m/s.

4.1.2 Complete model

The complete model is shown in Figure 4.2. It is built as for the CAD design with some adjust during assembly. Standard aeronautical safety wire is used to link the servomotor to the equilibrator arms. This let us reduce the clearance during movements since a pre load is possible during locking.

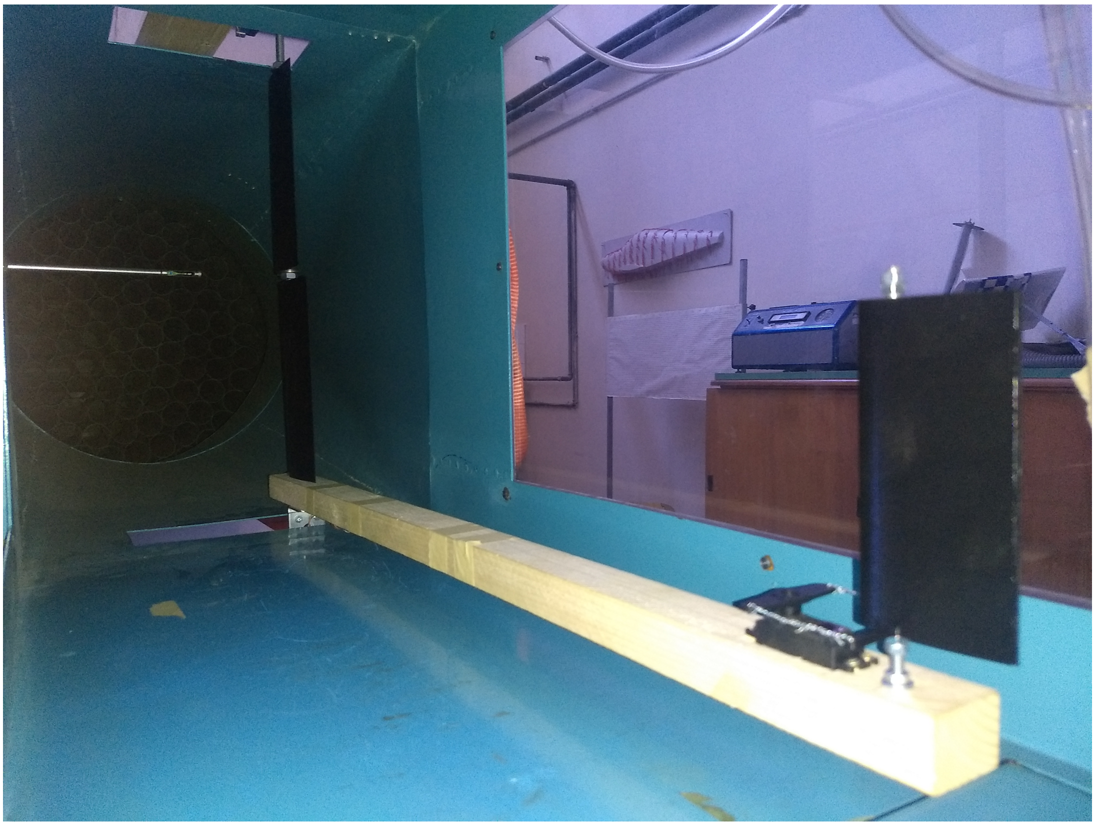

Figure 4.2: Test model assembly inside wind tunnel chamber.

4.1.3 Test balance

Lower part

The main part of the torsion balance is located at the bottom of the wind tunnel test chamber (Figure 4.3). A little welded frame was built to give a support to the balance. A wood table let screw the structure in arbitrary position.
On the joint there is the structure as for CAD design. During assembly we found that L support, originally designed to be fixed with four bolt and nuts, had to be screwed with two bolts only, for a collision problem. This causes some imprecision in measurements as we will see.

Upper part

The upper part of the balance consists in the bearing support and the third load cell. This is mounted on a big wooden joist fixed on the wind tunnel with belt. This was the best solution we found to not damage the wind tunnel plant and to have possibility to adjust position during assembly (Figure 4.4).

4.2 Test routine

Tests have been automatizated by a routine executed by two Arduino board linked to a laptop. `GNU Octave` was used to collect data and manage tests. The wind tunnel control system runs

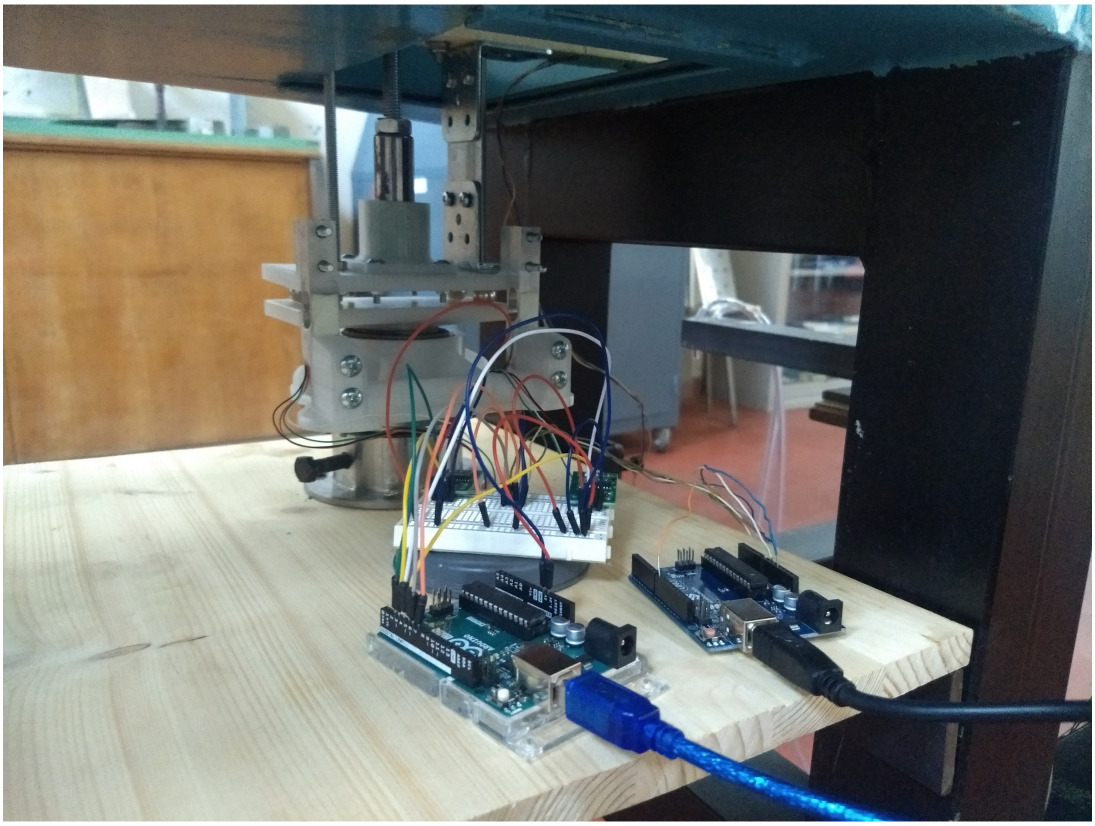

Figure 4.3: Test balance linked to electronic boards.

on a different PC and it is used to manage only the test chamber air speed.
Tests are done with a specific sequence that consist in:

- Choose a relative position between the fixed and the movable wing section, by inserting the threaded bar in one of the holes provided in the outer section.
- Choose an angle of attack and lock the bolt on the joint below the balance.
- Start the wind tunnel electric motor and set the control system to the chosen air speed. A variable time must be waited until the control system regulates the airspeed to the target with a tolerance.
- Start by Octave control the Arduino hardcoded routine. The equilibrator is moved to his highest angle of attach, then a closed loop control start to work. At every increasing step of the equilibrator, load cells value are read and the moment calculated. When the opportune moment is reached routine stop and the equilibrator angle is saved to a variable. Also totatal lift is saved. The other parameter is the torsional deformation angle reached by the outer section. It must be measured by a gauge fixed outside the wind tunnel. A photo of this gauge is taken from a fixed point. Under the gauge is fixed a graduated scale that provides a reference to make calculations and find the angle.

4.3 Possible improvements

During tests some problems occurred, and we found that some parts of the plant can be improved in some ways. In this section we describe this problems and the possible solutions for the future.

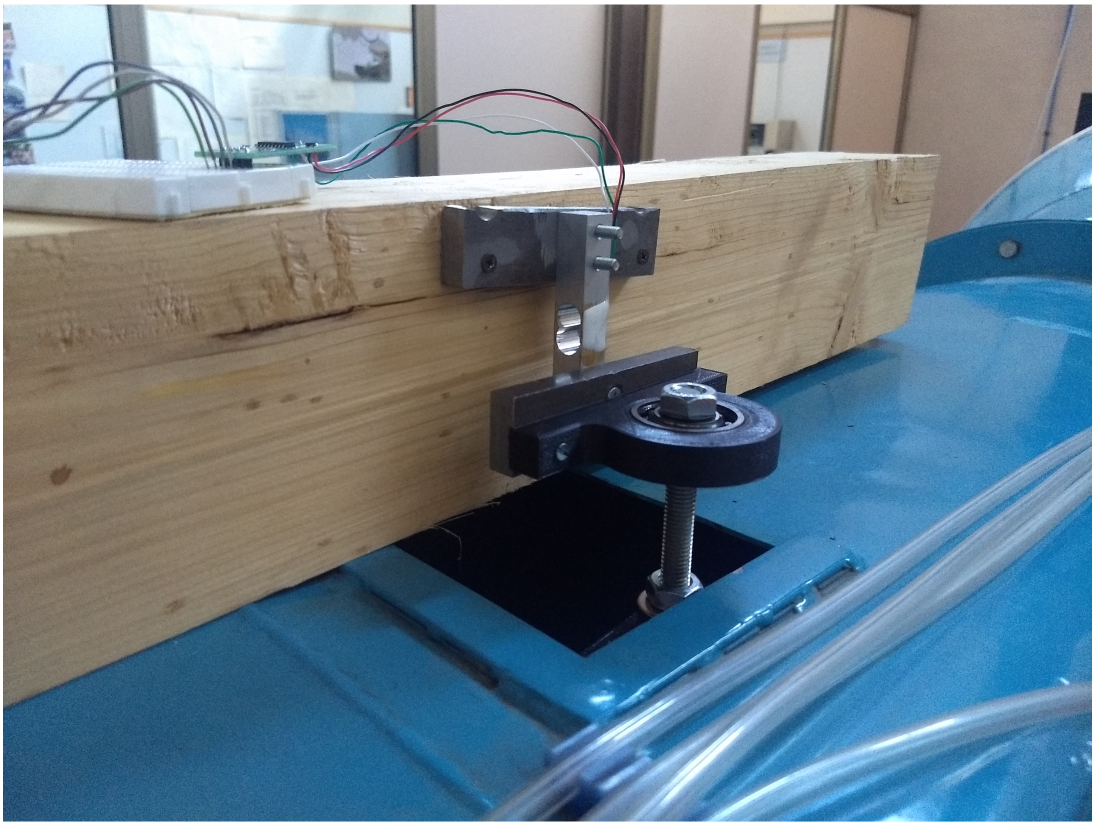

Figure 4.4: Linking system on the upper part of the load cell.

4.3.1 Test Balance

Construction

The test balance design can be improved moving one load cell to the opposite side. In this way there is an equal constrain on the two sides to keep closed the roller balls between the tables. Now the parallelism between the tables is very low, so the gap between balls is not constant and this can overconstrain the system. A metal construction for the structure should be taken into account to increase the stiffness and the precision in dimensions.
The balance rotate on a calibrated joint, that can be locked by a screw. This system can mantain the angle attack on a certain value, but it is very difficult to measure it, so it is not so sharp. This can be solved by a better joint with a screw driven gear system that can do little movements of the balance on high movement of the screw, and an opportune measuration system.

Load cells tare

Load cells must be tared with high precision. This is very important to avoid the rising of virtual moments due to a rough taring. As seen, the moment is measured by the difference of the force on the load cells times the harm between them. The torsional axe is (or should be) on the midpoint between cells. So a force applied in the midpoint should give a result on the Lift, but should not influence the Moment. Load cells produce an electric signal that is proportional to the applied force. So a constant must be found to transform tension [V] in a force [N]. This constant is a little bit different for each cell, depending on fabbrication and many more aspects. So, if this constant isn't so accurate, cells give, for the same load, results a little bit different. This leads to have a "virtual moment" that is not corresponding to a real torque on the balance but depends only on the characterization process.

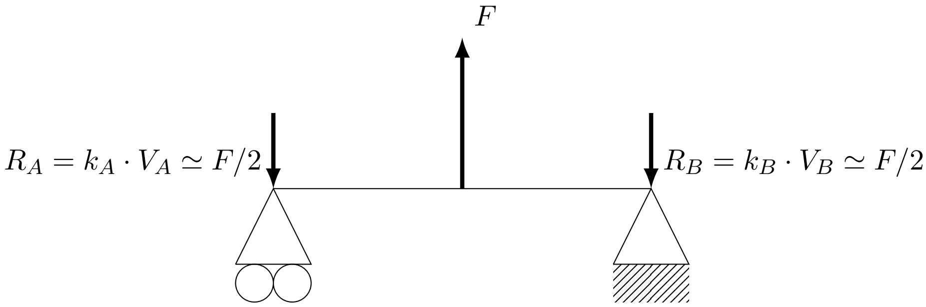

Figure 4.5: Schematization of the lower part of the balance. A force applied on the midpoint can even produce a virtual moment due to bad cells charaterization.

4.3.2 Elastomeric spring

The elastomeric spring is composed by an external support, in `petg`, an elastic part in rubber material and an internal steel support. The three parts are linked together by commercial epoxidik glue. Gluing is not a simple operation. The glue must be posed only on lateral cylindrical faces and not in other places. Moreover the distribution must be uniform but it is so difficult to obtain.
We also found that gluing can be acceptable to work in tests only for a limited during of time. Then the external support starts do detach from the rubber part in some point, so faces are not constrained together and the deformation becomes non-linear. The internal support has a different behaviour. It stay attacched to the rubber for a time, and then detach completely and fastly, so it becomes unusable.
A more efficient glue and gluing procedure must be studied.

4.3.3 Body

The body is composed by a wooden joist. The first problem with it is the flexibility. The flexibility of the fuselage is a problem also in reality, and NACA studies took it into account. For our theoretical model the fuselage is perfectly rigid so also in the test model should be. The second problem is the aerodynamic interference of his roughly squared shape.
A carbon fiber tubular should be studied to provide a stiff structure with a rounded shape.

4.3.4 Equilibrator

The equilibrator actuation system has a very simple kinematic design. The problem here is that all the construction is external and the aerodynamic interference with the equilibrator rises up. Considering to build a tubular structure for the body, as said, the actuation system could be studied to be inside the shape.
Morevoer the angular position of the equilibrator is chosen giving a signal to the servomotor that should rotate to the commanded position. The effective reaching of this position depends also from from the aerodynamic load on the section. Theoretically the stall force of the servomotor is by far higher the aerodynamic load, but to be shure, an indipendent position encoding system should be studied.

Chapter 5

Results Comparision

This section show a comparision between the results of the theoretical model and wind tunnel tests.
The comparision is done adjustyng entry data of the theoretical model. This is acceptable because some data are not known or they are difficult to measure.
In effects C_L of the different wing section has been reduced to 3 for the two main wing sections and to 2 for the equilibrator. This seems to be accetable considering the low aspect ratio, the aerodynamic interference caused by nuts, joists and other squared pieces.
The air density results to be a little lower than standard. This is explicable considering the wind tunnel architecture. This is a closed loop wind tunnel so there is little or no air shuffling. This leads to an air temperature increasing.
The stiffness of the elastomeric hinge was estimated in about 13 $\frac{N \cdot m}{rad}$. This is the value of the spring alone, but the rest of the model is not perfectly rigid, so the total stifness used in the model should be reduced to 3 $\frac{N \cdot m}{rad}$.
For what has been said the theoretical Lift and Deformation graph fits the experimental correspondants. The big difference comes out in the equilibrator angle graph.
A remark should be done about this. The link between the body (the wooden joist) and the torsion balance is done by a screwed L support. This was at first supposed to be locked with four screws but a problem during assembly occured. So we mounted the support in reverse position and only two screws. This increased the allowance between the two parts.
For the test routine, the equilibrator starts from the upper limit and, under the electronic board control, continue to decrease his angle of attack until the reach of the searched moment on the torsion balance. This leads to an inversion of sign on the moment that the equilibrator loads on the body. In this change of sign there is a displacement of the body equal to the clearance. This is the most reasonable cause of the error.

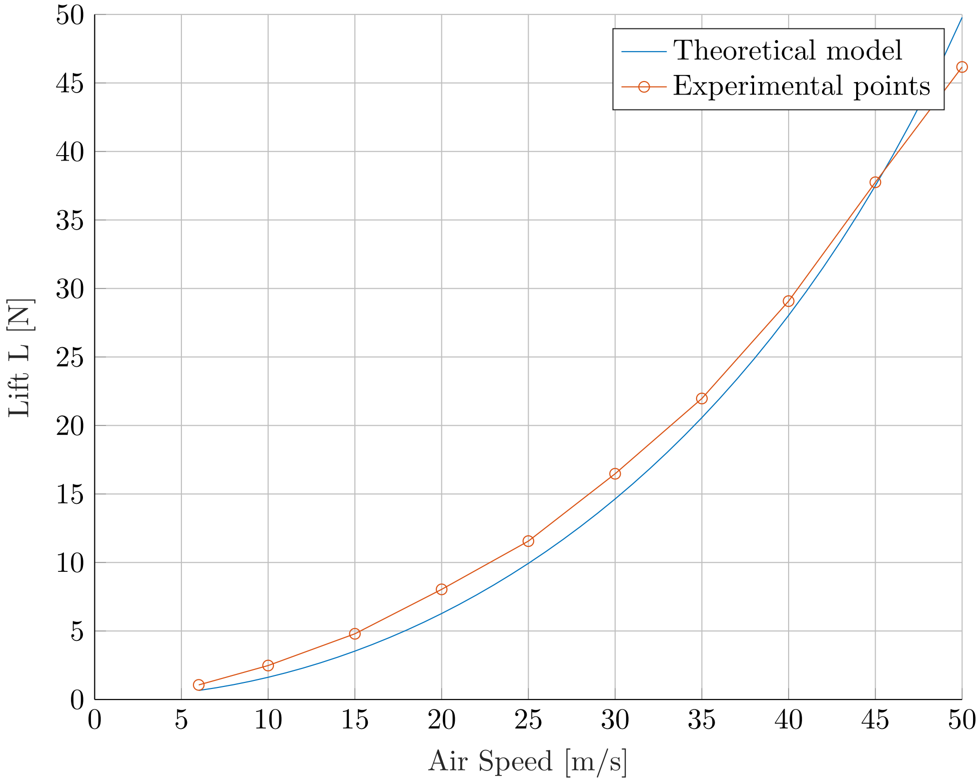
Theoretical model
Experimental points
Lift L [N]
Air Speed [m/s]
0
5
10
15
20
25
30
35
40
45
50

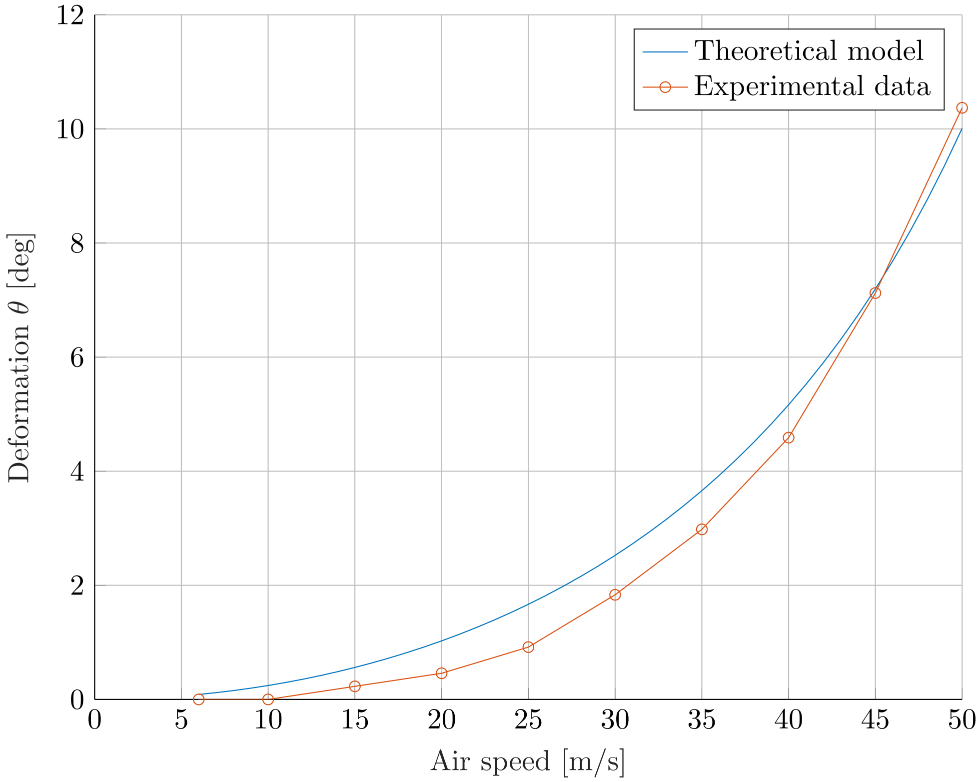
Theoretical model
Experimental data
Deformation θ [deg]
Air speed [m/s]
0
2
4
6
8
10
12
0
5
10
15
20
25
30
35
40
45
50

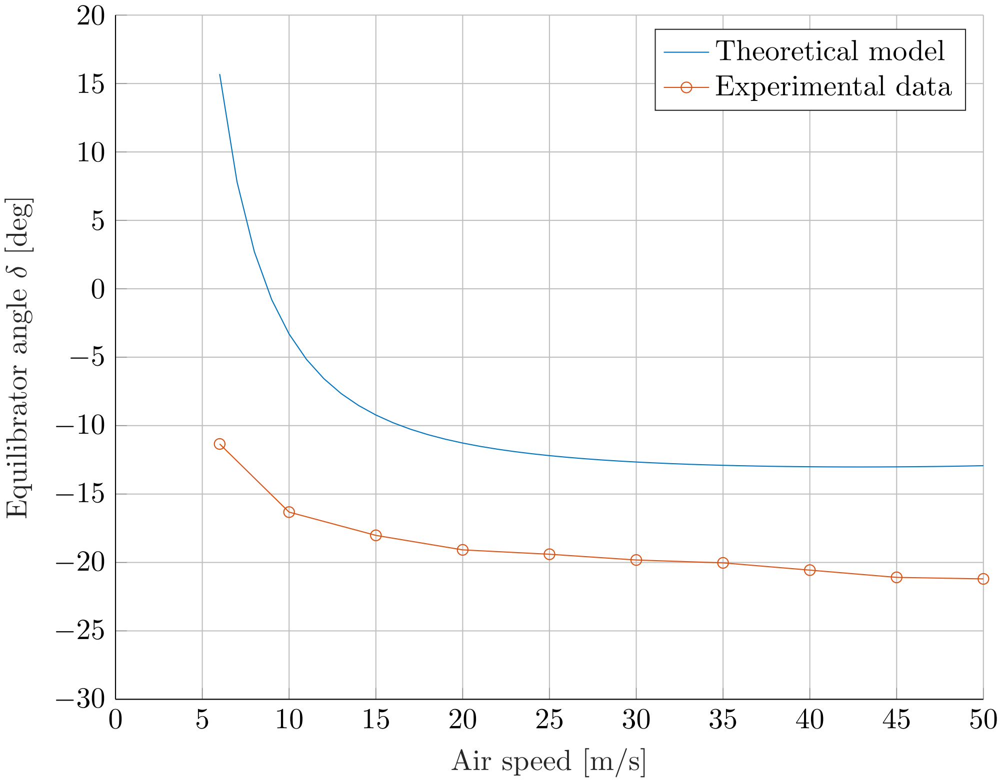
Theoretical model
Experimental data
Equilibrator angle δ [deg]
Air speed [m/s]
20
15
10
5
0
−5
−10
−15
−20
−25
−30
0
5
10
15
20
25
30
35
40
45
50

Appendix A

Source Code

A.1 Numerical Model

A.1.1 Data

```
%%
%Dati
% La superficie A è la parte interna della semiala, rigida.
% La superficie B è la parte esterna della semiala, calettata alla
   molla
% La superficie T è l'equilibratore

%Geometria Velivolo
XAac=0;                %[m]   Distanza dal datum del centro
   aerodinamico superficie A.
XBac=0.0125; %             %[m]   Distanza dal datum del centro
   aerodinamico superficie B.
XTac=0.9;                  %[m]   Distanza dal datum del centro
   aerodinamico superficie T.
cA=0.1;                    %[m]   Corda superficie A
cB=0.1;                    %[m]   Corda superficie B
cT=0.06;                   %[m]   Corda superficie T
bA=0.23;                   %[m]   Corda superficie A
bB=0.23;                   %[m]   Corda superficie B
bT=0.12;                   %[m]   Corda superficie T
SA=bA*cA;                  %[m^2] Estensione superficie A
SB=bB*cB;                  %[m^2] Estensione superficie B
ST=bT*cT;                  %[m^2] Estensione superficie T
W=1;
Xw=0.01;

%Coefficienti aerodinamici
CMA=0;                        %Coefficiente di momento superficie A
CMB=0;                        %Coefficiente di momento superficie B
CLAp=4;                       %Coefficiente angolare di portanza
   superficie A
CLBp=4;                       %Coefficiente angolare di portanza
   superficie B
```

```
CLTp=4;                        %Coefficiente angolare di portanza
   superficie T

%Molla
Xmol=0;                    %[m] Distanza dal datum dell'asse di
   cerniera tra A e B.
k=13.5441;                     %Coefficiente elastico della molla.

%Condizioni di volo
rho=1.225;                     %[kg/m^3] densità aria
Ve=6:1:55;                     %[m/s] velocità aria
qe=0.5*rho.*Ve.^2;             %[Pa] pressione dinamica
alpha=deg2rad(0:1:15);         %[rad] incidenza

plotpianta
```

A.1.2 Calculation

```
clear
close all
clc

dati

plotpianta

%%
%Calcolo

for i=1:length(qe)  %Coefficiente elastico della molla.
    q=qe(i);

    %Risposta aeroelastica superficie B
    theta(i,:)=(q*SB*cB*CMB + q*SB*CLBp*(Xmol-XBac).*alpha)./(k-q*SB*
       CLBp*(Xmol-XBac));


%Momento trasmesso da B ad A
    MBA(i,:)=q.*SB*cB*CMB + q.*SB*CLBp*(Xmol-XBac).*(alpha+theta(i,:)
       );

    %Momento superficie A nel suo fuoco
    MA(i,:)=q*SA*cA*CMA;

    %Portanza della superficie B
    LB(i,:)=q*SB*CLBp.*(alpha+theta(i,:));

    %Portanza della superficie A
    LA(i,:)=q*SA*CLAp.*(alpha);

    %Momento globale ala isolata
    Mwing(i,:)=MBA(i,:)+MA(i,:)-(Xmol-XAac).*LB(i,:);
```

```


    %Portanza che deve essere generata dall'equilibratore
    LT(i,:)=(Mwing(i,:)+W*(Xw-XAac))/(XTac-XAac);

    %Portanza totale

    L(i,:)=LA(i,:)+LB(i,:)+LT(i,:);

    %Angolo di deflessione dell'equilibratore
    delta(i,:)=(LT(i,:)-q*ST*CLTp.*alpha)./(q*ST*CLTp)+alpha;

    end
postprocessing
postprocessing3D
```

A.1.3 Postprocessing

```
%discretizzazione
plotalfa=1;
plotVe=4;

figure
hold on
for i=1:plotVe:length(Ve)
    plot(rad2deg(alpha),rad2deg(delta(i,:)))
end
hold off
title('Equilibratore')
xlabel('Incidenza \alpha [deg]')
ylabel('Deflessione \delta [deg]')
matlab2tikz('incdefl.tex','width','0.75\textwidth')

figure
hold on
for i=1:plotVe:length(Ve)
    plot(rad2deg(alpha),rad2deg(theta(i,:)))
end
hold off
title('Svergolamento')
xlabel('Incidenza \alpha [deg]')
ylabel('Svergolamento \theta [deg]')
matlab2tikz('sverginc.tex','width','0.75\textwidth')

figure
hold on
for i=1:plotVe:length(Ve)
    plot(rad2deg(alpha),(L(i,:)))
end
hold off
title('Portanza')
xlabel('Incidenza \alpha [deg]')
```

```
ylabel('Portanza L [N]')
matlab2tikz('portinc.tex','width','0.75\textwidth')

figure
hold on
for i=1:plotalfa:length(alpha)
 plot(Ve,rad2deg(theta(:,i)))
end
hold off
 title('Svergolamento/Velocità')
 xlabel('Velocità [m/s]')
 ylabel('Svergolamento \theta [deg]')
 matlab2tikz('svergvel.tex','width','0.75\textwidth')

 figure
hold on
for i=1:plotalfa:length(alpha)
 plot(Ve,rad2deg(delta(:,i)))
end
hold off
 title('Equilibratore/Velocità')
 xlabel('Velocità [m/s]')
 ylabel('Equilibratore \delta [deg]')
 matlab2tikz('eqvel.tex','width','0.75\textwidth')

 figure
hold on
for i=1:plotalfa:length(alpha)
 plot(Ve,L(:,i))
 %legend('\alpha=%s',alpha(i))
end
hold off
 title('Portanza/Velocità')
 xlabel('Velocità [m/s]')
 ylabel('Portanza L [N]')
 matlab2tikz('portvel.tex','width','0.75\textwidth')

  figure
 [x,y]=meshgrid(rad2deg(alpha),Ve);
  surf(x,y,L)
  xlabel('\alpha')
  ylabel('Ve')
  zlabel('L')

 figure
 [x,y]=meshgrid(rad2deg(alpha),Ve);
  contour(x,y,L,[W W])
  xlabel('\alpha')
  ylabel('Ve')
  zlabel('L')
```

A.1.4 3D Postprocessing

```
A=dlmread('dorso.txt',' ',0,1);
B=dlmread('ventre.txt',' ',0,1);

corda=4;

xu = A(:,1)';
yu = A(:,2)';
xl = B(:,1)';
yl = B(:,2)';


x =[xu, xl(end:-1:1)];
y = [yu, yl(end:-1:1)];

figure('Position', get(0, 'Screensize'))
aa=surf([cA*x+(XAac-0.25*cA); cA*x+(XAac-0.25*cA)], [cA*y; cA*y], [0*
    ones(size(x)); bA*ones(size(x))],'FaceColor','y');
hold on
bb=surf([cB*x+(XBac-0.25*cB); cB*x+(XBac-0.25*cB)], [cB*y; cB*y], [bA
    *ones(size(x)); (bA+bB)*ones(size(x))],'FaceColor','g');
cc=surf([cT*x+(XTac-0.25*cT); cT*x+(XTac-0.25*cT)], [cT*y; cT*y], [0*
    ones(size(x)); bT*ones(size(x))],'FaceColor','r');
pp=plot3((XTac), 0, 0,'*');
mm=plot3((Xmol), 0, 0,'*r');
tt=plot3([XAac XTac],[0 0],[0 0]);
plot3((XAac), 0, 0,'*b');
rr=plot3(cT*x+(XTac-0.25*cT),cT*y,zeros(length(x)),'w');%'b per
    vedere la traccia dell'equilibratore con ala rigida
     hold off
%view([-1 1 1])
view([0 0 1])


grid on

ind=length(Ve);
title('Vista dall''alto')
alf=rad2deg(alpha(2)-alpha(1));
teta=rad2deg(theta(ind,2)-theta(ind,1));
delt=rad2deg(delta(ind,2)-delta(ind,1));

for i=1:length(alpha)
    axis equal

     rotate(aa,[0 0 1],-(alf),[XAac 0 0])

     rotate(bb,[0 0 1],-(alf), [XAac 0 0])
     rotate(bb,[0 0 1],-(teta), [get(mm, 'xdata') get(mm, 'ydata') 0])
     rotate(cc,[0 0 1],-(alf), [XAac 0 0])

```

```
    rotate(cc,[0 0 1],-(delt), [get(pp, 'xdata') get(pp, 'ydata') 0])
    rotate(rr,[0 0 1],-(alf), [XAac 0 0])
    rotate(rr,[0 0 1],-(-0.6), [get(pp, 'xdata') get(pp, 'ydata') 0])
    rotate(pp,[0 0 1],-(alf), [XAac 0 0])
    rotate(mm,[0 0 1],-(alf), [XAac 0 0])
    rotate(tt,[0 0 1],-(alf), [XAac 0 0])

    legend(sprintf("\\alpha=%.1f",rad2deg(alpha(i))))

     pause(0.01)
end
% pause(2)
 title('Vista assonometrica')
 view([-1 1 1])
 axis equal
```

A.2 Data Acquisition

A.2.1 Octave acquisition automation

```
clear
close all
clc
pkg load instrument-control
disp("Prove salvate:")
ls ./prove
N=input("Inserire numero della nuova prova: \n");
clc
disp(["prova NÂ°",num2str(N)])
anc=1;
i=0;
while anc==1
i++;


V(i)=input("Inserire velocitÃ  aria della prova in m/s (Invio dopo
   averla raggiunta):\n");
clc
disp(["prova NÂ°",num2str(N),", velocitÃ  ",num2str(V(length(V)))," m
   /s"])
disp("Attendere ricerca angolo equilibratore")

if (exist("serial") != 3)
    disp("No Serial Support");
endif


s1 = serial("/dev/ttyACM0");
pause(1);

set(s1, 'baudrate', 9600);
set(s1, 'bytesize', 8);
```

```
set(s1, 'parity', 'n');
set(s1, 'stopbits', 1);
set(s1, 'timeout', -1);

srl_flush(s1);
read_back = ReadToTermination(s1);
a=str2num(read_back);
delta(i)=a(1);
L(i)=a(2);
M(i)=a(3);

fclose(s1);
clear s1
clc
disp(["prova NÂ°",num2str(N),", velocitÃ  ",num2str(V(length(V)))," m
   /s"])
disp(["Angolo equilibratore ",num2str(delta(length(delta))),"Â°,
   Portanza ",num2str(L(length(L)))," N"])

datval=yes_or_no("Dato valido?");
if datval==0
  i--;
endif
anc = yes_or_no ("Nuova velocitÃ ?");
clc
endwhile




%Salvataggio
sav=yes_or_no("Procedere al salvataggio?");
if sav==1
save (["./prove/prova",num2str(N)])
end
clc
```

A.2.2 Test data postprocessing

```
clear
close all
clc
disp("Prove salvate:")
ls ./prove
N=input("Inserire numero della prova da elaborare:\n");
clc
load (["./prove/prova",num2str(N)])

if (exist("theta","var")==0)
for k=1:length(V)
  disp(["prova NÂ°",num2str(N),", velocitÃ  ",num2str(V(k))," m/s"])
  mm(k)=input("Inserire mm indicatore theta\n");
```

```
  clc
endfor
theta=asind(mm./250);
save (["./prove/prova",num2str(N)])
endif

figure
plot(V,delta)
xlabel("V [m/s]")
ylabel(" \delta [Â°]")

figure
plot(V,L)
xlabel("V [m/s]")
ylabel("L [N]")

figure
plot(V,theta)
xlabel("V [m/s]")
ylabel("\theta [Â°]")
```

A.2.3 Arduino Code

```
#include "HX711.h"
#include <Servo.h>
#include <EEPROM.h>

Servo myservo;

#define DOUT1  3
#define CLK1   2
#define DOUT2  5
#define CLK2   4
#define DOUT3  7
#define CLK3   6

HX711 scale1(DOUT1, CLK1);
HX711 scale2(DOUT2, CLK2);
HX711 scale3(DOUT3, CLK3);

float calibration_factor1 = -193510;
float calibration_factor2 = -375820;
float calibration_factor3 = -420000;
int pos=1297;
float posagg;
float cella1;
```

```
float cella2;
float cella3;
float tara1;
float tara2;
float tara3;
float M=0;
float Mref=-0.1;
float soglia=0.02;
float P=0;



void setup() {
  Serial.begin(9600);
  myservo.attach(8);
  myservo.writeMicroseconds(pos); //circa 30 gradi
  scale1.set_offset(EEPROM.get(0,tara1));
  scale2.set_offset(EEPROM.get(sizeof(float),tara2));
  scale3.set_offset(EEPROM.get(sizeof(float)*2,tara3));
  scale1.set_scale(calibration_factor1);
  scale2.set_scale(calibration_factor2);
  scale3.set_scale(calibration_factor3);
}


void loop() {
  if(Serial.available())
  {
    char temp = Serial.read();
    if(temp == 't')
    myservo.writeMicroseconds(1580);
    scale1.tare(); //Reset the scale to 0
    scale2.tare();
    scale3.tare();
    tara1=scale1.get_offset();
    tara2=scale2.get_offset();
    tara3=scale3.get_offset();
    EEPROM.put(0,tara1);
    EEPROM.put(sizeof(float),tara2);
    EEPROM.put(sizeof(float)*2,tara3);
    Serial.print("Taratura eseguita");
    Serial.println(tara1);
    Serial.println(tara2);
    Serial.println(tara3);

    while (1)
  {
delay(1000);
  }
  }
  cella1=scale1.get_units();
```

```
  cella2=scale2.get_units();
  cella3=scale3.get_units();

M=(cella1-cella2)*0.12*9.81;
P=(cella1+cella2+cella3)*9.81;

 if (abs(M-Mref) > soglia && pos<1863)
 {
 pos++;
 myservo.writeMicroseconds(pos);
delay(10);
 }
else
{
 posagg=-float(pos-1580)*0.106;
  Serial.print(posagg);
  Serial.print("  ");
  Serial.print(P, 6);
  Serial.print("  ");
  Serial.print(M,6);
  Serial.println();
  while (1)
  {
delay(1000);
  }
}


}
```

Appendix B

Techical drawings

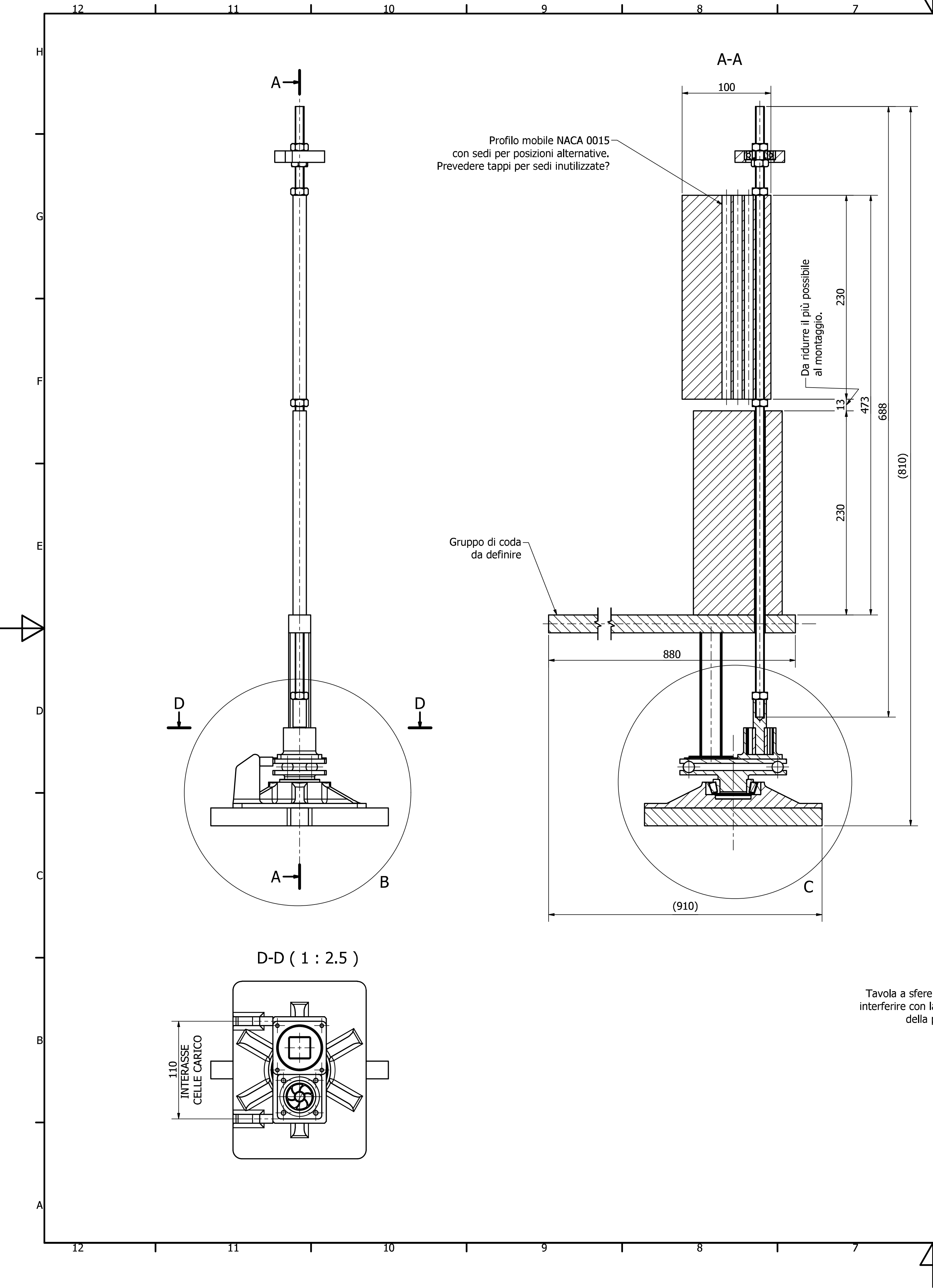
A-A
100
Profilo mobile NACA 0015
con sedi per posizioni alternative.
Prevedere tappi per sedi inutilizzate?
Da ridurre il più possibile
al montaggio.
230
13
473
688
(810)
230
Gruppo di coda
da definire
880
(910)
A
A
B
C
D
D
D-D (1 : 2.5)
110
INTERASSE
CELLE CARICO
Tavola a sfere
interferire con l
della
12
11
10
9
8
7
H
G
F
E
D
C
B
A

B (1:1)

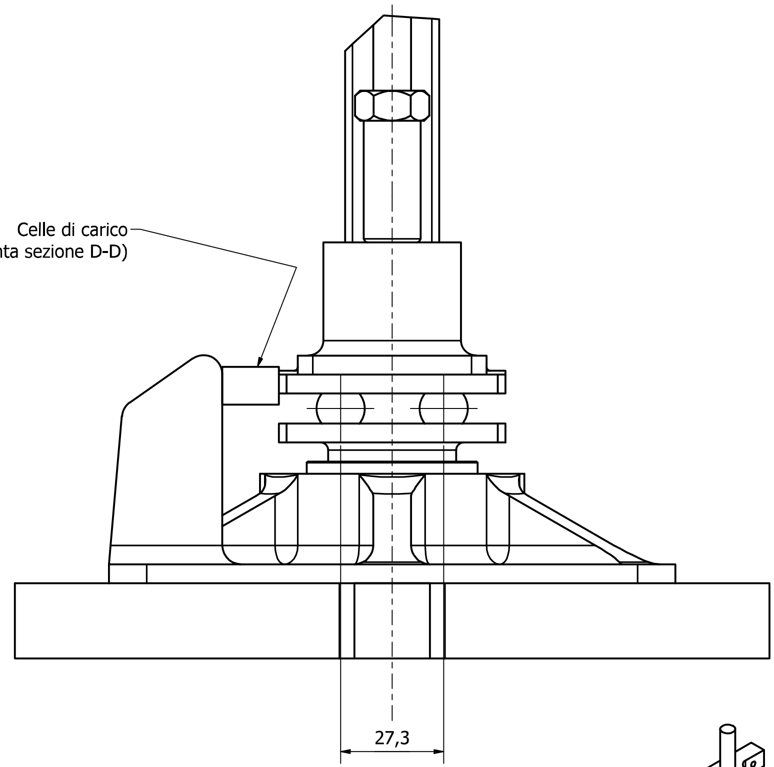

C (1 : 1)

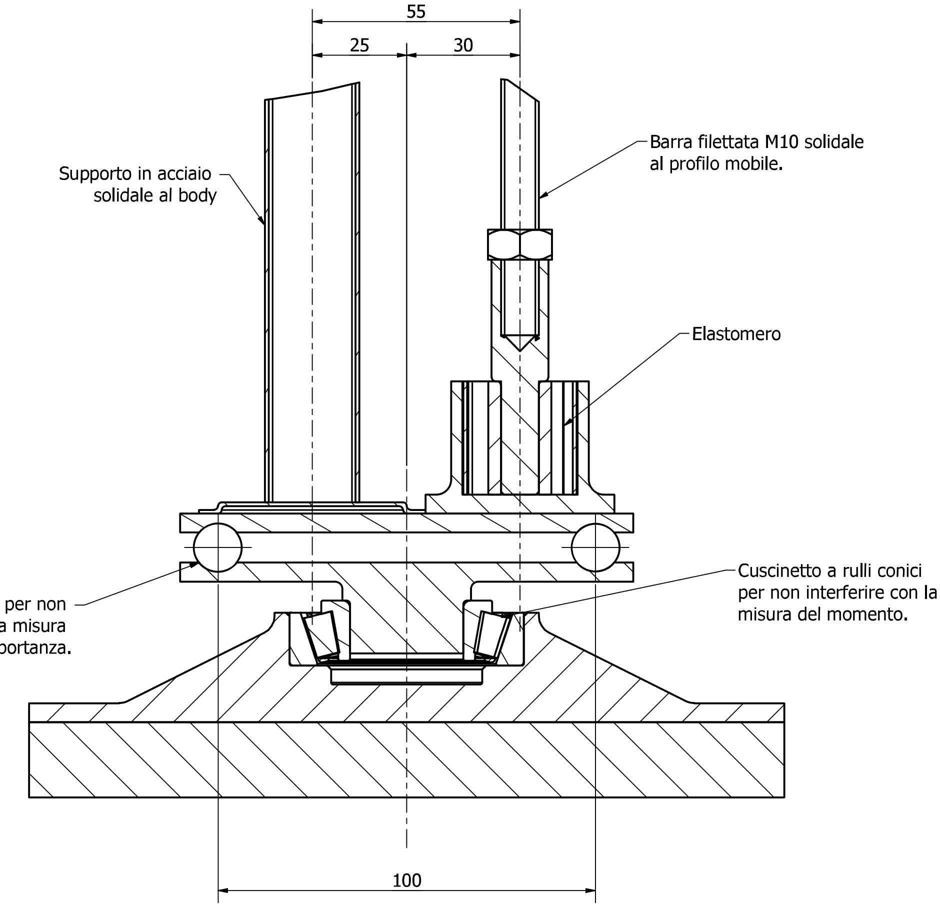

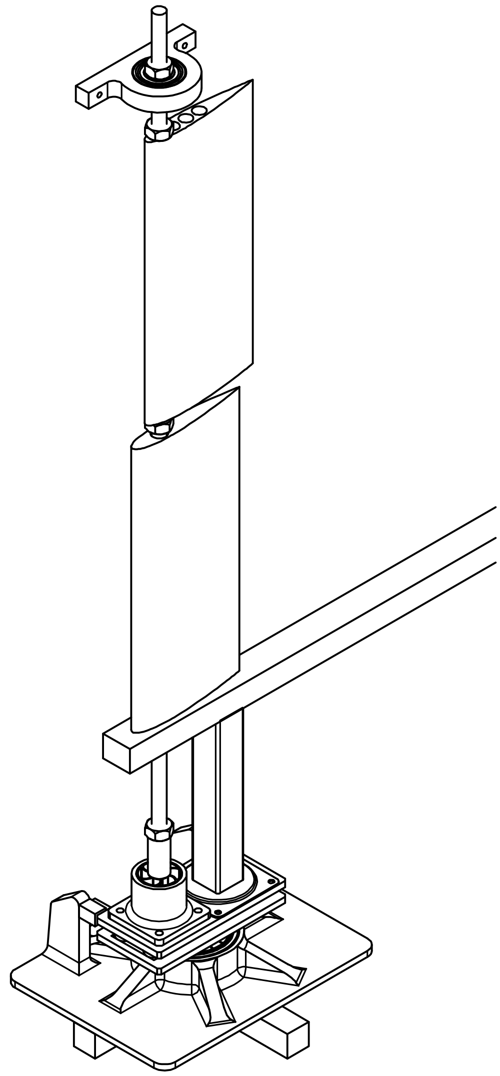

Progettato da	Controllato da	Approvato da	Data	Data
F. Pagano				02/12/2018
	Bilancia di Torsione		Edizione	Foglio 1 / 1

List of Figures

Acknowledgements

Many thanks to the high school I attended, I.T.I.S. A. Volta of Alessandria, that allowed me to use the wind tunnel and all the techical instrumentation. My thanks expecially go to the Volta Aeronautical Section rappresented by the teachers Simone Gatti and Leonardo Ferrazzi and to the school headmaster Maria Elena Dealessi.
A very special thank to Marcello Parodi and Riccardo Sacchi for the precious help building the 3D printed models and to Stefano Uggioni for machinings on wood.
Thanks to Federico Cucinella for the support programming Arduino.
Thanks to PGS s.r.l. expecially in the person of Luigi Rizzo for the precious advices about the experimental model designation.
I would like to thank the hardware shop "Cabella 2" for all the patience with me on strange components requests.